Computational predictions of energy materials using density functional theory

Anubhav Jain[1], Yongwoo Shin[1] and Kristin A. Persson[1,2]

Abstract | In the search for new functional materials, quantum mechanics is an exciting starting point. The fundamental laws that govern the behaviour of electrons have the possibility, at the other end of the scale, to predict the performance of a material for a targeted application. In some cases, this is achievable using density functional theory (DFT). In this Review, we highlight DFT studies predicting energy-related materials that were subsequently confirmed experimentally. The attributes and limitations of DFT for the computational design of materials for lithium-ion batteries, hydrogen production and storage materials, superconductors, photovoltaics and thermoelectric materials are discussed. In the future, we expect that the accuracy of DFT-based methods will continue to improve and that growth in computing power will enable millions of materials to be virtually screened for specific applications. Thus, these examples represent a first glimpse of what may become a routine and integral step in materials discovery.

In 1929, the physicist Paul Dirac wrote, "The underlying physical laws necessary for the mathematical theory of a large part of physics and the whole of chemistry are thus completely known, and the difficulty is only that the exact application of these laws leads to equations much too complicated to be soluble" (REF. 1). Since then, many new developments in physics, such as the creation of quantum electrodynamics (which traces back to Dirac's work), have underscored the reality that much of fundamental physics remains to be discovered. However, we expect that today's chemists and materials scientists would still largely agree with Dirac's sentiment. The physical laws governing the behaviour of a material are encapsulated in the Schrödinger equation[2]; however, if approached directly, this equation is intractable for realistic materials. To understand the difficulty of the problem, consider that 1 gram of any material contains on the order of 10^{23} electrons. Solving the Schrödinger equation for this system using a computer would require approximately 1 billion petabytes (10^{24} bytes) of computing space simply to represent the 3 spatial coordinates of each electron. Even if that obstacle could be circumvented and it were possible to build a computer capable of solving 10^{28} electron interactions per second, a period equivalent to the age of the universe would still be required to solve the ~10^{46} pairwise electron interactions in the system. Thus, there is no reason to assume that applying the laws of quantum mechanics to real materials should be simple. Instead, the best and often only way to probe the properties of materials is through experimentation and measurement.

Fortunately, the situation for computational materials scientists is not as hopeless as it seems. Many materials form crystal structures that can be represented by small, repeating units, much in the same way as tilework or carpet may consist of a single tessellating pattern. A macroscopic quantity of Si, for example, can be well approximated by a unit cell containing only 2 atoms (16 electrons). The resulting perfect crystal is a very good approximation of a real Si wafer used in electronics, which may contain only one defect per billion atoms. This considerable reduction of electrons, coupled with advancements that allow chemists to explicitly simulate only valence electrons, enable techniques such as quantum Monte Carlo to be performed using today's most powerful computers to solve the fundamental laws of quantum mechanics and subsequently predict the properties of materials[3]. However, quantum Monte Carlo techniques are time consuming, costly and currently intractable for all but the simplest materials. A more practical theory is needed for 'everyday use'.

Hohenberg, Kohn and Sham developed such a theory in density functional theory (DFT)[4,5], which has resulted in two of the top-ten cited papers of all time[6] and for which Kohn received the Nobel Prize in Chemistry in 1999. DFT reformulates ground-state

[1]*Environmental Energy Technologies Division, Lawrence Berkeley National Laboratory, Berkeley, California 94720, USA.*
[2]*Materials Science and Engineering Department, University of California Berkeley, Berkeley, California 94704, USA.*

Correspondence to K.A.P.
kapersson@lbl.gov

Article number: 15004
doi:10.1038/natrevmats.2015.4
Published online 11 Jan 2016

solutions to the Schrödinger equation as a problem of minimizing energy as a functional of the charge density (BOX 1). Although the exact energy functional has not been determined, approximate models for this functional have yielded accurate predictions for many classes of materials. Thus, many of the problems once lamented by Dirac have now been circumvented, thereby allowing the physical laws of quantum physics to be connected to the technologically relevant properties of materials. Facilitated by the exponential increase in computing power, DFT has led to a paradigm change in computational materials science, whereby theorists are not only able to help explain and interpret the properties of materials but also have an active role in predicting completely new materials with specific properties for different applications.

Box 1 | **What is density functional theory?**

Density functional theory (DFT) reformulates the Schrödinger equation, which describes the behaviour of electrons in a system, such that approximate solutions are tractable for realistic materials. The theory was first developed in 1964 by Hohenberg and Kohn[4], who determined that all ground-state properties can be cast as a functional of the charge density that must be minimized in energy. Rather than tackle the Schrödinger equation[2] head-on, these theorems suggested that one could instead iteratively improve on an initial guess of the charge density. Next, Kohn and Sham[5] paved the way for practical applications by recasting the fundamental equations to collect the most complex electron interactions in an 'exchange-correlation' functional. The exact form of this exchange-correlation functional remains unknown; however, approximations to it based on electron gas models and further extensions have proved successful for many classes of materials.

The choice of exchange-correlation functional determines, to a large extent, the accuracy of the DFT calculation. Although theorists can often improve the accuracy of calculation (typically at greater computational expense) through the use of more complex functionals[110], highly correlated electron systems exist for which most functionals fail. Other limitations[111,112] of standard DFT include the small system size (today's computers and DFT codes can routinely tackle periodic unit cells containing approximately 1,000 atoms or fewer), difficulty in modelling weak (that is, van der Waals) interactions, dynamics over long time periods and properties that are not ground state (that is, finite temperatures or excited states). However, methods for overcoming these limitations are often available; for example, larger systems can be tackled by the linear scaling approach[113], finite-temperature effects can be addressed through lattice dynamics[114] and cluster expansion[115], electronic excitations can be modelled using time-dependent DFT[116,117], the GW method[118] and the Bethe–Salpeter[119] technique, and several approaches can model van der Waals interactions[120]. A short discussion of some of these possibilities can be found in a review by Carter[121].

The inputs of a DFT calculation include, the coordinates and identities of the atoms in the material within a repeating lattice, the exchange-correlation functional, parameters and algorithms for numerical and iterative convergence, and, optionally, a method for more efficiently treating the core electrons in the system (for example, through the use of pseudopotentials). DFT produces output quantities such as the electronic charge density, total energy, magnetic configuration and electronic band structure. Most often, one must perform additional analysis to derive technologically useful properties from these fundamental ingredients.

As shown in the figure, many important materials properties can be determined through total energy calculations. For example, by computing the energy difference between the perfect crystal and a point defect, one can evaluate the thermodynamic properties of defects. Alternatively, one can evaluate energy differences along an atom's migration path to determine the energetics of diffusion barriers. By displacing atoms and analysing the resulting force in the remaining atoms, one can determine the phonon modes of the system and thereby derive properties such as the vibrational heat capacity. As a final example, by calculating the response to deforming the unit cell, one can probe the elastic properties of a material or obtain an equation of state. Other properties, such as the magnetic state, can also be evaluated through total energy evaluations.

DFT results are also used as descriptors[16] that are fed into scaling relations[41,122] or heuristics such as the Sabatier principle, which has been used with much success in the catalysis field[123]. In the past few decades, the use of DFT techniques to interpret and predict the properties of materials has grown tremendously because of the availability of easy-to-use computer codes (both commercial and open source), faster and more stable mathematical algorithms for solving DFT equations, and low-cost and widely available computing resources. Today, materials databases that contain the results of tens or hundreds of thousands of such calculations are publicly available[124–127] and are making DFT results accessible to both theorists and experimentalists.

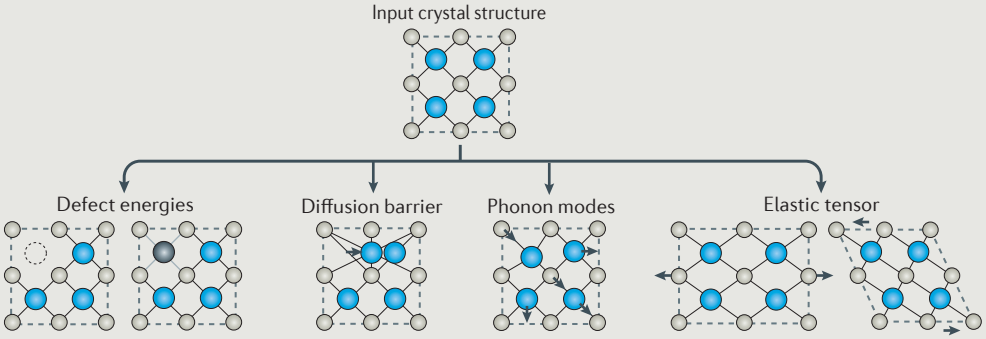

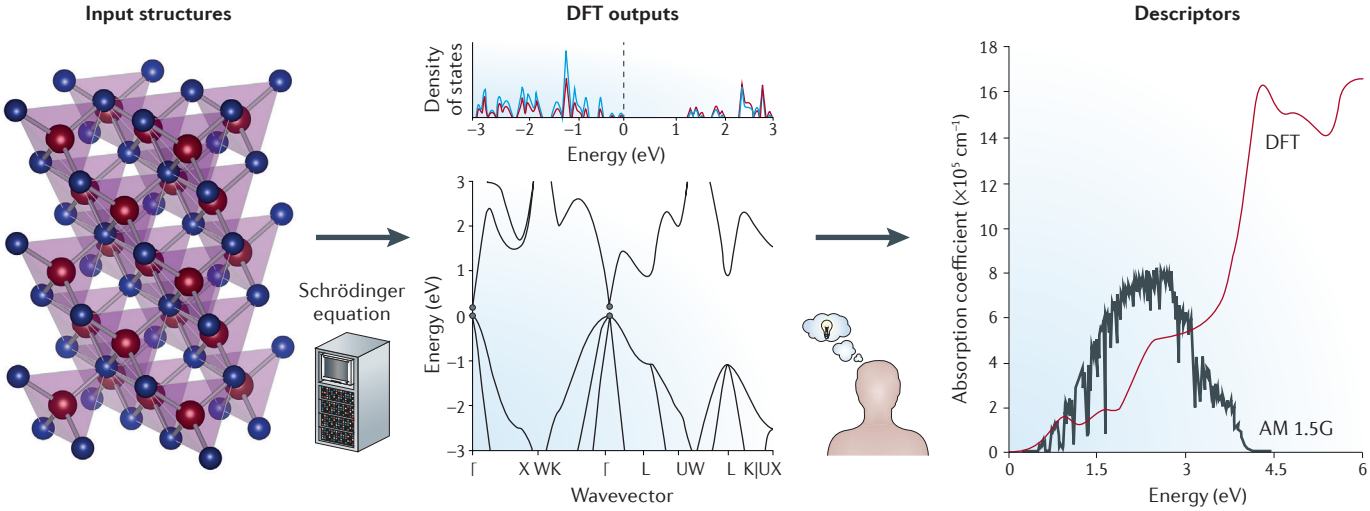

Figure 1 | **Procedure to screen for materials properties using density functional theory calculations.** The calculations require, as an input, a reasonable estimate of the crystal structure (periodic unit cell and atomic positions) of the proposed material or molecule, along with a choice of approximations and numerical convergence parameters. The output of the density functional theory (DFT) calculation yields fundamental quantities such as the electron charge density, total energy, optimized crystal structure and band structure. The fundamental outputs from DFT must be analysed or combined to produce descriptors relevant to a given application. For example, a version of the optical absorption can be related to the joint density of states and wavefunction overlap integrals. Knowledge derived from DFT calculations often determines the next set of compounds that are tested.

In this Review, we detail case studies from this new world of materials design. We concentrate only on examples where theoretical prediction has led to the experimental discovery of a new material or exposed an important technological facet of a known material. The examples chosen are restricted to materials for renewable energy applications, which are a major focus in DFT-based materials discovery. Examples from other applications, including magnetic materials and multiferroic materials, can be found elsewhere[7–9]. Similarly, we do not cover studies that use methods other than DFT, such as atomistic force fields[10–14]. Our goal is not to be comprehensive but rather to employ selected examples as a platform for discussing the current state of the art in computational materials discovery. Finally, we discuss some themes that are common to many of the examples presented and provide an outlook for the future of DFT in materials design.

In silico materials design

Although the outputs of a DFT computation provide important fundamental attributes of a material, the path to a technological quantity of interest is rarely direct. As phrased by Gerbrand Ceder, "there is no quantum operator for a better car" (REF. 15). Rather, *in silico* design involves several stages, which progress from computation to insight (see FIG. 1 for a description of these stages). A major component of this process is translating the fundamental physical outputs from DFT into knowledge that is practically useful for an application using the principles of materials science and domain-specific expertise[16]. To illustrate how this procedure works in practice, we discuss in the following sections several examples for which DFT was used to target technological applications.

Lithium-ion batteries. These batteries are currently the dominant technology for consumer electronics and next-generation electric vehicles. In the late 1990s, pioneering work was carried out by Ceder and co-workers[17–19], who related the outputs of DFT calculations to the technological attributes of battery electrodes. One of the first properties to be determined for electrode materials was the expected voltage, which determines the energy stored per unit charge. Ayindol *et al.*[17] related this quantity to the total energy difference between the electrode crystal structures at different states of charge (that is, containing variable amounts of Li). After making this crucial connection, it became straightforward — with careful treatment of electron localization[20] — to predict voltages in hypothetical electrode materials. For example, Ceder *et al.* predicted that by doping Al into a layered $LiCoO_2$ cathode material, the voltage could be raised; this was then borne out experimentally[18].

Similarly, frameworks for connecting DFT-computable quantities to other battery-material properties, such as ionic diffusion, phase stability and thermal safety, were developed[21–23]. Computations of the energy barrier required to migrate a Li ion could be used to guide the optimization of materials and improve the power delivered by Li-ion batteries. For example, Kang *et al.*[24] computed the effect of $LiMn_{0.5}Ni_{0.5}O_2$ layer spacing on Li-ion migration barriers, finding that even small expansions of the layer spacing should produce significant improvements in Li diffusivity. They were subsequently able to synthesize the desired material (FIG. 2a) by the ion exchange of Li for Na in $NaMn_{0.5}Ni_{0.5}O_2$, which resulted in samples with lower Li–Ni disorder and thereby larger layer spacing. At high charging rates, the samples prepared using the

modified synthesis technique greatly outperformed those prepared using the conventional synthesis route (FIG. 2b), demonstrating the ability of DFT-based design to tune materials for high-power batteries. Similar techniques were recently used by Ong *et al.*[25] to develop new solid-state electrolytes that avoid the use of Ge.

One further step was taken by Jain *et al.*[26] in developing automation software to virtually screen very large numbers of new electrode materials in a 'high-throughput' mode before beginning experimental testing. Using this methodology, Ceder and co-workers screened thousands of cathode materials and identified and experimentally verified several of them, including a monoclinic form of $LiMnBO_3$ (REF. 27), layered $Li_9V_3(P_2O_7)_3(PO_4)_2$ (REF. 28) and Cr-doped $LiVO_2$ (REF. 29). One interesting case study is a new class of $Li_3MPO_4CO_3$ (M = transition metal) materials, which are unconventional in that they mix two different polyanion groups (phosphate and carbonate). They were 'invented' by automatic element substitution algorithms[30,31] applied to all the relevant crystal structures in the Inorganic Crystal Structure Database (ICSD)[32], which revealed that a Na-to-Li substitution in natural sidorenkite minerals could yield potential battery cathodes. Thus, using a similar strategy to that previously described for $LiMn_{0.5}Ni_{0.5}O_2$, Na-containing carbonophosphates were prepared hydrothermally followed by an ion-exchange process, which resulted in the desired Li analogues[33]. The Li-containing carbonophosphates, with a general formula, $Li_3MPO_4CO_3$, could be synthesized with various transition metals in the M site[34], and the computations indicated that the choice of transition metal greatly influences the electrochemical properties. Of particular interest was $Li_3MnPO_4CO_3$, for which computations predicted a possible exchange of two Li cations per Mn cation. However, further optimization of this system is required owing to a potentially incomplete Na–Li ion-exchange process. Natural sidorenkite minerals are also candidates for cathodes in next-generation Na-ion batteries[35,36], in which case no ion-exchange procedure is required.

Apart from cathodes, computations have also been used to help identify 2D anode materials. Anasori *et al.*[37] performed DFT computations to predict the atomic ordering of 20 new 2D carbide materials, known as MXenes. One of these materials, $Mo_2Ti_2C_2T_x$, where T represents a surface termination, was synthesized and tested for electrochemical activity, yielding modest performance as a potential anode material that can possibly be further tuned by exploring different compositions within the MXene family.

Hydrogen production and storage. Hydrogen fuel can reach very high energy densities[38], but cost of production, storage and conversion to electricity remain obstacles that have thus far limited its application. The development of new materials holds promise for improving the economics of using hydrogen as a fuel, and computations are one pathway towards identifying such compounds.

The first step in using hydrogen as an energy storage medium is its production. Hydrogen can be generated from natural gas or other hydrocarbons through a process known as steam reforming. In a study published in 1998, Besenbacher *et al.*[39] used DFT to predict that detrimental graphite build-up on Ni catalysts for steam reforming could be inhibited by alloying with Au and verified the result experimentally. The study was an early demonstration that new materials for catalysis could be explored with DFT. Further work in catalysis for hydrogen production was conducted by Greeley *et al.*[40], who

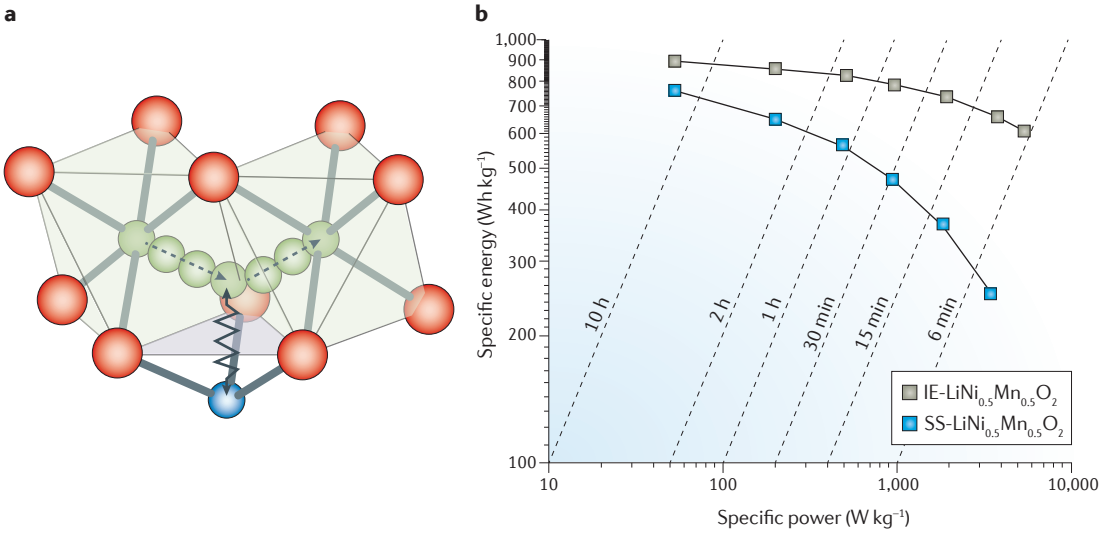

Figure 2 | **Computational design of high-rate-capability Li-ion battery materials. a** | The diffusion path of Li ions (green) through a lattice of oxygen (red) and transition metal ions (blue). By computing activation barriers of this diffusion path as a function of layer spacing, Kang *et al.*[24] proposed a novel ion-exchanged cathode material to improve rate capability. **b** | An experimental Ragone plot, which demonstrates the superior performance of the ion-exchanged (IE) material compared with a conventional solid-state (SS) material in maintaining high energy densities during high-power cycling. Adapted with permission from REF. 24, American Association for the Advancement of Science.

studied cheaper alternatives to Pt for catalysing the electrolysis of water (a second way to produce hydrogen). They screened a library of 256 candidate alloys, encompassing a matrix of substrate and solute metals, for compounds that would efficiently catalyse the hydrogen evolution reaction ($2H^+ + 2e^- \rightarrow H_2$). Because catalysis is difficult to model directly, the authors used the Sabatier principle to relate binding energies to catalytic behaviour[41]. Crucially, they also included stability metrics that screened out several materials that otherwise exhibited good calculated performance. The study resulted in the identification of Bi–Pt alloys as potentially cheaper materials that retain the high performance of pure Pt in experiments[40]. This study was one of the first to demonstrate that DFT could be used to screen libraries of compounds for 'hits', and it also helped to establish that stability (and not just calculated performance) is an important criterion to ensure that DFT predictions are relevant to experiments. A final example comes from Yan *et al.*[42], who explored photocatalytic materials for water splitting (that is, using sunlight to convert H_2O to H_2 and O_2). They screened hundreds of transition metal oxides and selected $Mn_2V_2O_7$ as a possible candidate based on a detailed assessment of the bandgap, band edge position with respect to O_2/H_2O and H_2/H^+ levels, and stability in aqueous environments (that is, Pourbaix analysis). Experimental characterization within the same study confirmed a stable photocurrent at high pH values, which was consistent with the calculations, but also revealed that a co-catalyst was needed for efficient oxygen evolution. It is worth noting that stability was again a major criterion, and, in this case, the authors were able to use a newly developed formalism for computing Pourbaix diagrams[43] to add aqueous stability to their screening criteria.

Once produced, hydrogen can be stored in several ways: for example, as a compressed gas, as a liquid or embedded within a solid compound. This last method has been the subject of several DFT investigations[44–46], and in 2006 Alapati *et al.*[47] demonstrated that it was possible to identify new compound mixtures for hydrogen storage. They studied the thermodynamic hydrogenation enthalpy of over 100 possible reactions, searching for new examples within a target range of 30–60 kJ mol^{-1}. A material with a 1:1 ratio of $LiNH_2$ and MgH_2 was identified as a possible candidate from the computations. Subsequent experiments confirmed the hydrogenation energy to be within 4 kJ mol^{-1} of the computational prediction and also demonstrated a hydrogen storage capacity of 8.1 wt%[48,49]. Interestingly, the capacity and the hydrogenation mechanism of the material are very sensitive to the ball milling method used, which initially led to conflicting experimental reports[48–51]. This example illustrates that although DFT can accurately predict the performance of a new material, it usually cannot determine the processing conditions needed to achieve the theoretical performance in practice.

Superconductors. Superconductivity remains one of the most elusive materials properties to predict from theory. Not only does it originate from several different physical phenomena, but the root cause of the resistance-free flow of electricity in some classes of materials is still not completely understood[52]. Superconducting materials are frequently divided into 'traditional' superconductors, in which the crucial electron-pairing interaction stems from electron–phonon coupling, and 'new' superconductors (for example, copper oxides and iron oxides), in which proximity to magnetic fluctuations is essential. For traditional superconductors, theory has not only provided the means to explain the observed phenomena[53–55], but it has also been used to predict new materials that have subsequently been synthesized and verified experimentally.

The earliest computational prediction of a superconducting material is remarkable as it was made when DFT was in its infancy. In 1984, Chang and Cohen[56] observed an anomalously high electron density at the Fermi level in pressurized Si and speculated that the material may become superconducting under such conditions. One year later, the prediction was confirmed when superconductivity was observed in Si below 8.2 K at 15 GPa (REF. 57). Similarly, Liu and Cohen[58], Neaton and Ashcroft[59], and Christensen and Novikov[60] predicted superconductivity for several new polymorphs of Li as a function of pressure. These predictions were also verified shortly afterwards by several independent research groups[61–63] for pressures above 20 GPa and temperatures below 20 K. In 2010, Kolmogorov *et al.*[64] predicted a superconducting temperature (T_c) of 15–20 K for orthorhombic high-pressure FeB_4, which was subsequently synthesized above 8 GPa and exhibited superconductivity below 3 K under ambient conditions[65] (FIG. 3). Recently, the sulfur hydrides have gained interest as potential superconductors at high pressure; however, pinpointing the exact phase responsible has remained elusive owing to extensive polymorphism and issues relating to phase stability. In 2014, Li *et al.*[66] predicted the likely onset of superconductivity by pressure-induced phonon softening and metallization in *P*1 and *Cmca* sulfur deuteride (H_2S) above 100 GPa and at temperatures below 80 K. Following this prediction, H_2S was confirmed as a superconductor at a remarkable temperature and pressure of 203 K and 90 GPa, respectively, albeit with some uncertainty as to which phase in the H–S system is responsible for the superconducting properties[67].

One challenge highlighted by these examples is polymorphism: many materials exhibit several phase transformations as a function of pressure that are not known in advance. Accurate crystal structure prediction therefore becomes a necessary step to correctly calculate the properties of a material (BOX 2). For example, high-pressure silane (SiH_4) was speculated[68] to exhibit superconductivity at very high pressure; however, its structure was unknown. Although the superconductivity of this system has not been fully verified[69], Pickard and Needs[70] successfully predicted a stable structure at 250 GPa, which was subsequently confirmed by experiments[71].

Theory has made a tremendous contribution to the field of superconductivity by providing a framework with predictive capability for traditional superconductors. For

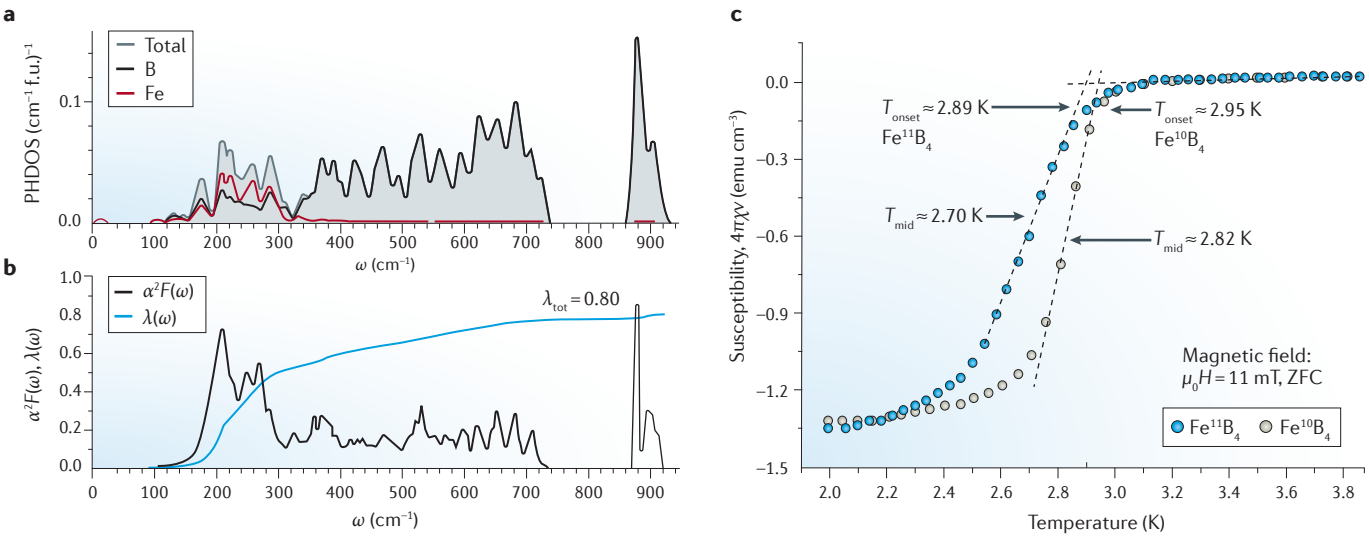

Figure 3 | **Prediction of superconductivity in FeB_4. a** | Phonon density of states (PHDOS). **b** | Eliashberg function, $\alpha^2F(\omega)$, where F is the density of vibrational modes and α is the electron coupling constant (black) and electron–phonon coupling strength, $\lambda(\omega)$, where ω is the phonon frequency (blue), in the $P10$ phase of FeB_4 calculated by Kolmogorov and co-workers[64]. **c** | Two sets of magnetic susceptibility data (for samples enriched with ^{10}B and ^{11}B isotopes) on FeB_4, measured in an applied field of 1 mT (zero-field cooling, ZFC) by Gou and colleagues[65]. f.u., formula unit; T_{mid}, superconducting transition midpoint temperature; T_{onset}, superconducting transition onset temperature. Panels **a** and **b** adapted with permission from Kolmogorov, A. N., Shah, S., Margine, E. R., Bialon, A. F., Hammerschmidt, T. and Drautz, R., *Phys. Rev. Lett.* **105**, 217003 (2010). Copyright (2010) by the American Physical Society. Panel **c** adapted with permission from REF. 65. Copyrighted by the American Physical Society.

Fe and Cu oxides, a comprehensive theory was presented only days after their original discovery[52]. Although applications of superconductors traditionally appeared only in specialized areas, such as particle colliders, superconducting materials are now being utilized for grid voltage and power stabilization (for example, dynamic volt–amp reactive (DVAR) systems). To further increase the scope of their application, an increased superconducting temperature (T_c) and lower manufacturing costs are required. Although superconductivity remains a property that may be easier to measure than to compute, we expect that as the theory for the new classes of superconductor matures, efficient computational techniques to screen for novel compounds with higher T_c will be developed.

Photovoltaics. Although the use of photovoltaics (PVs) for energy generation is increasing rapidly (with an almost 125-fold growth in the US energy capacity from 2003 to 2013)[72], their contribution to total electricity generation remains small. Several classes of PV materials are being actively investigated, including single-crystal, amorphous and polycrystalline Si, III–V compounds, thin-film chalcogenides, organic photovoltaics (OPVs) and multijunction devices[73]. DFT methods to screen inorganic compounds have been developed[74], but thus far have only been applied to known classes of compounds[75]. Here, we focus specifically on OPVs, which became feasible following the discovery of the first organic semiconductor, *trans*-polyacetylene[76], and subsequent 'second-generation' discoveries[77,78]. OPVs are attractive because of their potentially low cost and light weight; however, they suffer from low power conversion efficiencies and short lifetimes[79]. In 2006, Mühlbacher *et al.*[80] proposed a new idea for designing organic semiconductors using copolymers, which are considered as third-generation organic semiconductors[81]. Copolymers comprise two monomer units that exhibit different electronic structures and geometries. Using this principle, researchers developed various organic semiconductor materials to achieve target electronic properties, including those for OPVs. However, designing these materials from first principles is not straightforward because standard DFT does not accurately model the electron localization of π-conjugated systems[82]. In addition, conventional conducting polymers contain tens to hundreds of atoms in a single chain and are thus too large to apply typical post-Hartree–Fock approaches. Other theoretical models and approximations of DFT must be applied[83–85]. As examples, the Harvard Clean Energy Project applied a single point calculation on various optimized geometries using several different functionals[86]; Körzdörfer and Brédas[87] applied hybrid functionals to organic electronic materials; and Sokolov *et al.*[88] developed a computational screening procedure to discover new organic semiconductors for organic field-effect transistors.

In 2007, Blouin *et al.*[89] computationally screened derivatives of poly(2,7-carbozole) as potential OPVs through assessment of the following criteria: air stability, as evaluated by the position of the highest occupied molecular orbital (HOMO) energy level relative to air, a charge-transfer energy offset of the lowest unoccupied molecular orbital (LUMO) at least 0.3 eV higher than

the acceptor level, and an optical bandgap between 1.2 and 1.9 eV. They calculated the properties of nine carbazole derivatives using DFT with the hybrid B3LYP exchange-correlation functional. Of these materials, six were selected for synthesis and characterization as thin films with phenyl-C_{61}-butyric acid methyl ester (PCBM) as the acceptor and a donor/acceptor ratio of 4:1 (FIG. 4). Measurements of the short-circuit current, open-circuit voltage and fill factor confirmed poly(*N*-9′-heptadecanyl-2,7-carbazole-*alt*-5,5(4′,7′-di-2-thienyl-2′,1′,3′-benzothiadiazole) (PCDTBT) to be the best potential donor material for OPV applications. The power conversion efficiency of the new material was measured to be 3.6%[89], and further optimization of the donor/acceptor ratio and morphology may be possible. In addition to the identification of a new material, the calculations helped to explain the trends observed among the six carbazole derivatives that were tested. The HOMO levels of all the derivatives were similar and fixed by the carbazole, whereas the inserted monomer units controlled the LUMO energy levels[89] (later confirmed by alternative computational methods[90]).

Another type of material applicable to PVs is transparent conducting films. Such materials are unique in that they simultaneously possess large bandgaps (required for transparency) and high electrical conductivity. Transparent conductive films are used in electronic devices (for example, touchscreen displays) and can be used as an alternative to wire-mesh current collectors in PV devices. One outstanding challenge in the development of transparent conductors is the discovery of suitable p-type conductors (that is, conductors that transport positively charged holes while remaining optically transparent). Two recent studies have tackled this problem using a high-throughput screening approach[91,92].

An initial study by Hautier *et al.*[91] screened over 3,000 compounds — focusing only on known oxides — for materials with a large bandgap and a low p-type effective mass. For selected candidates, more detailed computational assessments of dopability were also performed. One of the materials identified from the screening was Ba_2BiTaO_6, a rhombohedral double perovskite that possesses an atypical energy alignment between the Bi 6*s* and O 2*p* orbitals, resulting in higher mobilities through hybridization. This material was synthesized using solid-state techniques by Bhatia *et al.*[92], who confirmed the presence of high transparency (>90%) in the visible region and a high hole mobility (>30 $cm^2\ V^{-1}\ s^{-1}$), but reported a very low carrier concentration ($5 \times 10^{13}\ cm^{-3}$).

Another recent study by Yan *et al.*[93] focused on the high-throughput screening of both known and hypothetical half-Heusler ABX alloys. This study uncovered some general principles for the design of half-Heusler-based materials; for example, materials with a single transition metal are generally metallic, whereas those with two transition metals tend to be non-metals. These principles led to the identification of TaIrGe, which was synthesized and tested within the same study[93]. Similar to the previous case of Ba_2BiTaO_6, TaIrGe exhibits high visible light

Box 2 | **New compounds and structures predicted by density functional theory**

Knowledge of a material's crystal structure (that is, the spatial arrangement of its atoms) is essential for understanding its properties and is a prerequisite for performing density functional theory (DFT) computations. Experimental approaches, such as X-ray diffraction and nuclear magnetic resonance, are available to probe and ultimately solve a material's crystal structure. Alternatively, a computational approach can be used, which possesses obvious advantages: no physical sample is needed and extreme conditions (for example, high pressure) can be used. The principle underlying computational crystal structure prediction is energy minimization: that is, to identify the atomic arrangement that yields a global minimum in energy under the desired thermodynamic constraints[128]. Although a local optimization of the atomic coordinates within DFT is routine, finding the global minimum within the space of all possible crystal structures remains a daunting task[129].

Over the years, many approaches have been developed to tackle the problem of structure prediction. One popular and successful approach involves evaluating the energy of the candidates' crystal structures and selecting the lowest-energy candidate as the 'best guess' solution. Within this framework, several methodologies have been developed. One conceptually simple technique is random crystal structure prediction[130], which generates random arrangements of atoms (within sensible constraints on bond lengths) and uses local optimization to stabilize those arrangements. The advantages of this technique include simplicity, lack of bias and ease of parallelization; however, it may require many calculations to arrive at a good solution. A popular approach that offers better efficiency is to use evolutionary algorithms[131]. Such algorithms typically begin with random structures but improve candidate guesses over time by 'mating' the lowest-energy solutions found at every iteration[128]. Finally, some of the most efficient algorithms leverage statistics and data mining[31,132–135] to 'learn' crystallization rules based on large data sets, such as the Inorganic Crystal Structure Database[32]. However, a disadvantage of the data-mining approach is that it can introduce bias by producing compounds that are similar to those already observed, thereby missing new and exotic phases. A more recent method to improve efficiency is to use partial experimental information to enforce constraints on symmetry[136]. Each of these methods has its own niche for application. Examples of successful structure predictions include highly compressed ammonia[137–139], a transparent, dense form of sodium[140] and the ilmenite structure of $SnTiO_3$ (REFS 134,141).

Finally, we note that crystal structure prediction is not limited to solving the structure for compositions for which a compound is already known to exist. Amendments to this technique can be used to predict entirely new compounds for experimental exploration. One recent example is the computational prediction by Gautier *et al.*[142] of 54 new half-Heusler compositions, of which 15 compounds have already been experimentally synthesized and confirmed. Thus, DFT-based techniques have the potential to aid researchers in efficiently filling in the knowledge gaps for new and exciting compounds[134].

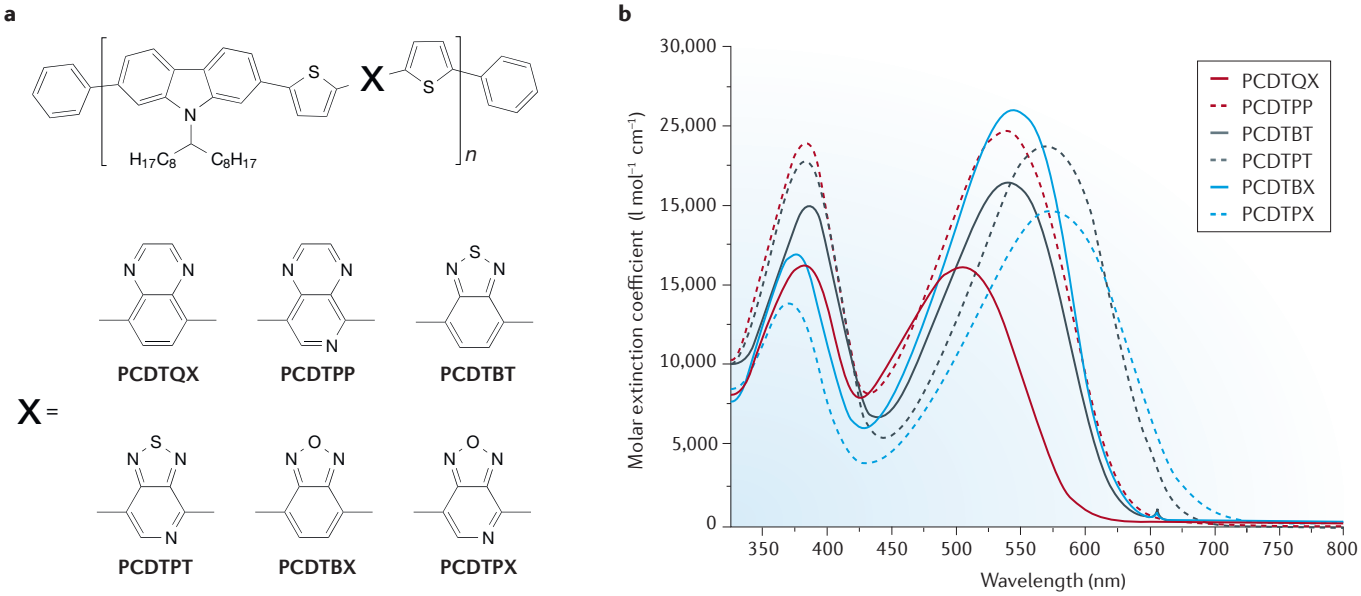

Figure 4 | **Screening of copolymers for organic photovoltaics. a** | Structures of the 2,7-carbazole-based alternating copolymers. **b** | UV–visible spectra at 135 °C in 1,2,4-trichlorobenzene. Adapted with permission from REF. 89, American Chemical Society.

transparency (in the range of 85–92%) as well as very high Hall mobilities (2,730 $cm^2 V^{-1} s^{-1}$). However, its low carrier concentration (8×10^{14} cm^{-3}) and the high cost of Ir are potential limiting factors that necessitate further optimization.

Thermoelectrics. Thermoelectric materials exploit temperature differences to drive electrical currents and vice versa. Potential applications of thermoelectric materials include waste heat recovery (from power generation plants and transportation vehicles) and refrigeration; however, commercialization has been minimal because of the relatively high cost and low efficiency of these devices.

To assess the intrinsic performance of thermoelectric materials, researchers typically employ a 'figure of merit' (or *ZT*), which is proportional to the temperature, electronic conductivity and Seebeck coefficient (the voltage generated per degree of temperature difference), and is inversely proportional to the thermal conductivity. Thermoelectric materials are challenging to design because there is an inherent trade-off between these quantities in almost all materials, which limits the *ZT* that can be attained. The use of phonon-glass electron-crystals and band alignment represent routes that circumvent the typical trade-offs[94,95]; however, these are applicable to only a small subset of materials.

Because it is difficult to estimate the quantities that determine the thermoelectric performance of a material, it would be useful to be able to compute such properties from first principles. Unfortunately, the computation of thermoelectric properties is often limited by theoretical shortcomings or computational expense. For example, estimations of the Seebeck coefficient and electronic conductivity are impeded by the difficulty of using DFT to produce accurate bandgaps and carrier lifetimes (that is, relaxation times). Furthermore, accurate treatment of the thermal conductivity is expensive and time consuming. The effects of high temperature on these properties can also be difficult to ascertain. Although almost all of these limitations can be overcome for simple materials and with careful and detailed study[96], it is not currently possible to perform such detailed calculations on a large scale or for highly complex materials.

Nevertheless, these challenges have not deterred computational searches for new thermoelectric materials. Rather, researchers frequently approximate many quantities in an effort to yield qualitative (but nevertheless predictive) trends that can be used to compare different materials with a relatively high degree of confidence. In 2006, Madsen[97] pioneered the use of computational search techniques for thermoelectric materials. The approximation had severe limitations: thermal conductivity was not modelled, the functionals used underestimated the bandgaps, and a constant and arbitrary relaxation time was used for electronic transport. Despite these known limitations, Madsen was able to recover known thermoelectric materials (such as skutterudites) in his screening and, crucially, also predicted new materials. One of the most promising materials predicted was an anisotropic n-type LiZnSb, which was calculated to have *ZT* in the range of 1.4–2.4 (depending on the approximations used). The LiZnSb material was subsequently synthesized by Toberer *et al.*[98] but could not be formed with n-type doping. Instead, the experiments indicated that LiZnSb was intrinsically p-type and possessed a much lower *ZT* of less than 0.1.

Despite the approximations used and not arriving at the desired material, the measured Seebeck coefficients showed remarkable agreement with those calculated

for the p-type material (FIG. 5). Rather, the problem seemed only to be that the desired material could not be synthesized with the correct carrier type. Indeed, Toberer *et al.*[98] noted the propensity of many materials similar to LiZnSb to form p-type compounds in the experimental literature. Thus, the limitation of the study[97] was not the overt and known approximations made during the screening process, but the implicit assumptions about dopability and carrier type, which were not considered at all. Nevertheless, Madsen's study triggered several other computational investigations into new thermoelectric materials[99,100]. For example, Zhu *et al.*[101] recently reported a $TmAgTe_2$ thermoelectric material discovered using high-throughput DFT with an experimentally measured *ZT* reaching 0.35. Furthermore, new formalisms for estimating thermoelectric properties[42] suggest that more computational predictions may be made in the near future.

Capacitors. A capacitor stores electrostatic energy through the polarization of an electric field within a material. There are many classes of capacitors corresponding to different mechanisms of polarization, including traditional dielectric capacitors, ferroelectrics, carbon-based supercapacitors and pseudocapacitors.

Taking dielectric capacitors as an example, the primary desirable properties include a high dielectric constant, high breakdown strength and excellent cycling stability. Sharma *et al.*[102] conducted an exhaustive search for novel dielectric polymeric materials by screening 1D repeat units for high dielectric constants (both ionic and electronic) using density functional perturbation theory and an effective medium theory[103,104]. Although the electronic component of the dielectric constant depended almost linearly on the bandgap, the ionic contribution showed no such dependence; this behaviour was exploited to maximize the dielectric capacity. Within the same study, three of the most promising candidates (none of which had been previously considered as a dielectric) were synthesized, with favourable agreement between the predicted and measured properties. This agreement was particularly good for polyurea $[–NH–CO–NH–C_6H_4–]_n$, which exhibited a dielectric constant of 5.4–5.8 and a dielectric loss at 1 kHz of 1%. However, one of the top materials identified, polythiourea, was experimentally observed to exhibit limited solubility and sensitivity to processing conditions. Hence, subsequent computational work explored chain derivatives and substitutions; this information was used in experimental investigations[105] towards improvement of the material. This work elegantly showcases the efficiency of combining computational and experimental techniques by leveraging the strengths of each domain. Although solubility and processing remain difficult to calculate accurately, the dielectric constant can be reliably estimated as a function of structural and chemical properties. Thus, rather than trying to perform the entire design *in silico*, the goal is almost always to focus the experimental efforts within a specific chemical and structural space.

Outlook

In this Review, we surveyed many successful examples of predicting materials for renewable energy using computations. Although not all case studies could be highlighted (see TABLE 1 for a more comprehensive list), the works discussed embody many of the overall principles for modern computational materials design. As demonstrated, many types of DFT prediction can provide guidance for experimental synthesis. In some cases, such as the high-throughput screening of battery

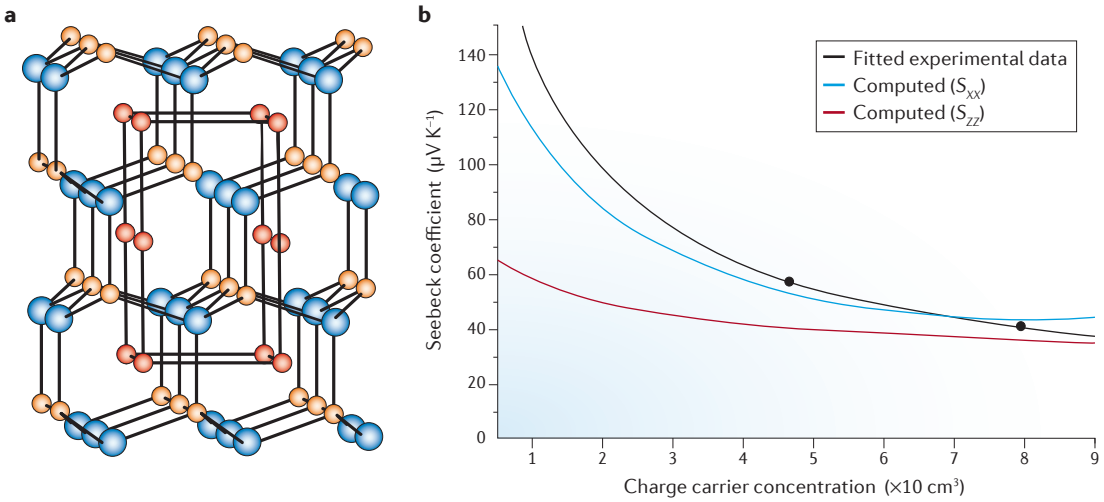

Figure 5 | **LiZnSb: a candidate thermoelectric material suggested by computation. a** | Wurtzite crystal structure of LiZnSb with Li interstitials. Sb, blue; Zn, orange; Li, red. **b** | Computed Seebeck coefficient (corresponding to two components of the Seebeck tensor, S_{XX} and S_{ZZ}) and fitted experimental data for p-type LiZnSb as a function of charge carrier concentration. The two data points represent different samples. Reprinted with permission from Toberer, E. S., May, A. F., Scanlon, C. J. and Snyder, G. J. Thermoelectric properties of p-type LiZnSb: assessment of *ab initio* calculations. *J. Appl. Phys.* **105**, 063701 (2009). Copyright 2009, AIP Publishing LLC.

cathodes resulting in sidorenkites, standard DFT can be used to predict many of the important properties of a material before it is selected for synthesis. This type of analysis is closest to a 'virtual screening' model, for which DFT calculations act as a cheap and scalable proxy for experimentation. However, in other cases, such as for thermoelectric LiZnSb, assumptions are inherent in the DFT analysis. In these cases, it is important to emphasize how the assumptions bias the results and at what level of accuracy the predictions should be trusted. For such cases, one can still use DFT in a qualitative way to guide experiments to yield

Table 1 | **Density functional theory predictions of energy-related materials that were confirmed by experiments**

Year	Material	Description	Refs
Li-ion batteries			
1998	$Li(Co_xAl_{1-x})O_2$	Al mixing to raise voltage	18
2006	$Li(Mn_{0.5}Ni_{0.5})O_2$	Li–Na ion exchange from the Na complex used to form the Li complex to improve Li–Ni ordering and achieve larger layer spacing	24
2011	$LiMnBO_3$	First use of the monoclinic phase as a cathode material	27
2011	$LiMPO_4CO_3$ (M = transition metal)	New class of sidorenkite-based cathode materials synthesized by Na ion-exchange	30,33,34
2012	$Li_9V_3(P_2O_7)_3(PO_4)_2$	New compound for cathodes	28
2012–2013	$Li_{10}SnP_2S_{12}$	New superionic conductor composition for solid-state electrolytes	25,143
2015	$Mo_2TiC_2T_x$ (2D)	2D material identified as an anode material; can also be used as a capacitor	37
Hydrogen production and storage			
1998	NiAu alloy	Catalyst for steam reforming to produce H_2 while preventing graphite build-up	39
2006	BiPt alloy	Cheaper and potentially better-performing H_2 production catalyst than pure Pt	40
2006–2010	$LiNH_2$:MgH_2 (1:1)	H_2 storage mixture; performance found to depend on ball milling procedure	47–49
2014	NiGa alloy	Catalyst that uses H_2 to reduce CO_2 into methanol as a liquid fuel, with lower production of CO than conventional Cu, ZnO and Al_2O_3 catalysts	144
2015	$Mn_2V_2O_7$	Solar water-splitting material; experiments showed photocurrent under specific electrochemical conditions but indicated that achieving efficient oxygen evolution will require a catalyst	42
Thermoelectrics			
2006	LiZnSb	n-Type compound suggested but only p-type could be synthesized	97
2006–2007	$FeSb_2$	Very high Seebeck coefficient and power factor achieved but low *ZT* because of high lattice thermal conductivity	106,107
2015	$TmAgTe_2$	Very low thermal conductivity achieved and moderate *ZT* (0.35) demonstrated, but impractical choice of elements	101
Photovoltaics			
2007	PCDTBT	Candidate copolymer donor material with high power conversion efficiency for bulk-heterojunction organic photovoltaic solar cells	89
2014	Organic dyes	New class of organic dyes for dye-sensitized solar cells	145
2013–2015	Ba_2BiTaO_6	p-Type transparent conducting oxide that utilizes alignment between Bi 6*s* and O 2*p* states	91,92
2014	TaIrGe	Unconventional p-type half-Heusler transparent conducting oxide composed of all heavy metal atoms	93
Superconductors			
1984–1985	Si (high-pressure)	Superconductivity hypothesized based on high density of states (DOS) near the Fermi level; superconductivity verified at 15 GPa and <8.2 K	56,57
1991–2003	Li (high-pressure)	Superconductivity verified at pressures above 20 GPa and temperatures <20 K	58–63
2010–2013	FeB_4 (high-pressure)	Orthorhombic *Pnmn* structure, synthesized at 8 GPa, shows behaviour indicative of superconductivity below 3 K and 1 atm	64,65
2014–2015	H_2S (high-pressure)	Predicted *P*1 or *Cmca* structure but unconfirmed by experiments; synthesized at 90 GPa, shows behaviour indicative of superconductivity at 203 K	66,67
Capacitors			
2014	Polymers for dielectric applications	267 polymers screened for dielectric constants and bandgaps; polyurea, polyimide and polythiourea synthesized with polyurea, in particular, showing very low dielectric loss	102
2015	Variants of polythiourea	Variation of the chemical design of polythiourea and experimental validation reaching a dielectric constant of 4.5 and energy densities of 10 J cm^{-3}	105

useful results. For example, the predictions of superconductivity were based largely on the examination of the computed density of states (DOS) and qualitatively searching for features thought to correlate with the target metrics. Such cases are common in the DFT literature; for example, Bentien *et al.*[106,107] realized that $FeSb_2$ should form a very-high-Seebeck-coefficient material based largely on correlating features of the computed DOS with known high-Seebeck-coefficient materials. Thus, the aim is not always comprehensive screening or the development of fully predictive models, but rather to accelerate the discovery process past the ability of experimentation alone. Sometimes, limitations of standard DFT that prevent a comprehensive virtual screening approach can be overcome through careful application of more exact methods. However, it is important to emphasize that attention to accuracy is never a substitute for relevance. For example, Madsen could have computed more accurate bandgaps for the predicted n-type LiZnSb material; however, such an effort would have been irrelevant as the subsequent experiment revealed LiZnSb to be p-type. Thus, it is often not the known approximations that derail a DFT prediction, but rather that some properties of the experimentally attainable material were not considered at all. It should also be noted that theoretical prediction is not always the most efficient route to obtain complete information about a material; often, calculations can be more time consuming and less straightforward than experiments. Interestingly, there seems to be little correlation between the difficulty of a measurement and a calculation. For example, the superconducting temperature (T_c) is still challenging to calculate despite being fairly straightforward to measure. By contrast, calculating single-crystal bulk ionic mobility is efficient compared with the experiments required. Therefore, it can be extremely beneficial to combine experimental and computational techniques, leveraging the best of both worlds as was demonstrated by the research groups of Ramprasad[102] and Sotzing[105] in the discovery and optimization of dielectric polymers.

A characteristic of the DFT approach that is both a strength and a limitation is its potential to compute scenarios outside the realm of nature. Even though this capability was detrimental to the thermoelectrics study conducted by Madsen, it enabled the more speculative study of the lattice-spacing effect on Li-ion mobilities pursued by Kang and colleagues[24]. Although the initial calculations for $LiMn_{0.5}Ni_{0.5}O_2$ with greater layer spacing were purely hypothetical, the calculations were nevertheless able to demonstrate the potential of such a material if it could be synthesized. Being able to easily control thermodynamic conditions without knowing the specifics of how they can be achieved experimentally is a tremendously important and often-neglected advantage of computations. The ability to answer 'what if' questions such as what if I can increase the layer spacing away from equilibrium, make the material defect free, reach 200 GPa, stabilize a metastable structure — and how these changes would affect the properties — can guide the experiments and pave the way towards rational design and optimization. Conversely, it can be difficult to distinguish when a computationally derived material and its associated properties are outside the realm of what is physically possible. It is all too easy for theorists to posit new materials that are impossible for experimentalists to make. Today, one can evaluate the decomposition energy of new compounds into known phases (an indicator of thermodynamic stability) and also assess the dynamical stability with respect to phonons. However, there remains a great need in the field to emphasize stability and to develop better methods to bridge the gap between computational prediction and successful synthesis.

Finally, it is important to point out that even with a high-throughput computational approach, the possible outcomes are bounded by the initial decision with respect to the chemical and structural space. For example, a major recent development in the PVs community is the hybrid organic–inorganic halide perovskite system[108,109]. Such materials were completely off the radar of computational studies, which had focused separately on inorganic or organic systems. Thus, even large-scale computational screening is certainly not exhaustive, and calculations will continue to be guided by experiments. Although the present method of using DFT to screen for new materials has strengths and limitations, it is important to point out that the capabilities of DFT continue to expand. For example, in the 10-year span from 2005 to 2015, the total computing capability of the top 500 computing systems has expanded by a factor of 200, from 1.7 to 363 PFlop s^{-1} (see Top500 website). This improvement, combined with more efficient and stable numerical algorithms for solving the equations, means that studies that were considered too computationally expensive just a decade ago are now being run routinely. Similarly, new methods for treating the limitations of DFT are being developed and packaged into stable and easy-to-use software libraries. Thus, it is an exciting time for theorists and experimentalists alike to leverage the new capabilities that DFT-based materials design has to offer.

1. Dirac, P. A. M. Quantum mechanics of many-electron systems. *Proc. R. Soc. Lond. A* **123**, 714–733 (1929).
2. Schrödinger, E. An undulatory theory of the mechanics of atoms and molecules. *Phys. Rev.* **22**, 1049 (1926).
3. Foulkes, W., Mitas, L., Needs, R. & Rajagopal, G. Quantum Monte Carlo simulations of solids. *Rev. Mod. Phys.* **73**, 33–83 (2001).
4. Hohenberg, P. & Kohn, W. Inhomogeneous electron gas. *Phys. Rev.* **136**, B864–B871 (1964).
This study established the theoretical basis of density functional theory.
5. Kohn, W. & Sham, L. J. Self-consistent equations including exchange and correlation effects. *Phys. Rev.* **140**, A1133 (1965).
This paper described the Kohn–Sham theorems that paved the way for practical implementations of density functional theory.
6. van Noorden, R., Maher, B. & Nuzzo, R. The top 100 papers. *Nature* **514**, 550–553 (2014).
7. Ceder, G. Predicting properties from scratch. *Science* **280**, 1099–1100 (1998).
8. Hafner, J., Wolverton, C. & Ceder, G. Towards computational materials design: the impact of density functional theory on materials research. *MRS Bull.* **31**, 659–668 (2006).
9. Hautier, G., Jain, A. & Ong, S. P. From the computer to the laboratory: materials discovery and design using first-principles calculations. *J. Mater. Sci.* **47**, 7317–7340 (2012).
10. Wilmer, C. E. *et al.* Large-scale screening of hypothetical metal–organic frameworks. *Nat. Chem.* **4**, 83–89 (2012).
11. Schmidt, J. E., Deem, M. W. & Davis, M. E. Synthesis of a specified, silica molecular sieve by using computationally predicted organic structure-directing agents. *Angew. Chem. Int. Ed. Engl.* **53**, 8372–8374 (2014).
12. Schmidt, J. E., Deem, M. W., Lew, C. & Davis, T. M. Computationally-guided synthesis of the 8-ring Zeolite AEI. *Top. Catal.* **58**, 410–415 (2015).

13. Bai, P. *et al.* Discovery of optimal zeolites for challenging separations and chemical transformations using predictive materials modeling. *Nat. Commun.* **6**, 5912 (2015).
14. Farha, O. K. *et al. De novo* synthesis of a metal–organic framework material featuring ultrahigh surface area and gas storage capacities. *Nat. Chem.* **2**, 944–948 (2010).
15. Ceder, G. Opportunities and challenges for first-principles materials design and applications to Li battery materials. *MRS Bull.* **35**, 693–701 (2010).
16. Curtarolo, S. *et al.* The high-throughput highway to computational materials design. *Nat. Mater.* **12**, 191–201 (2013).
17. Aydinol, M., Kohan, A., Ceder, G., Cho, K. & Joannopoulos, J. *Ab initio* study of lithium intercalation in metal oxides and metal dichalcogenides. *Phys. Rev. B* **56**, 1354–1365 (1997).
18. Ceder, G. *et al.* Identification of cathode materials for lithium batteries guided by first-principles calculations. *Nature* **392**, 694–696 (1998).
This paper presented the first demonstration that density functional theory could be used to practically tune the voltage of Li-ion battery electrode materials.
19. Van Der Ven, A., Aydinol, M. K. & Ceder, G. First-principles evidence for stage ordering in Li_xCoO_2. *J. Electrochem. Soc.* **145**, 2149–2155 (1998).
20. Zhou, F., Cococcioni, M., Kang, K. & Ceder, G. The Li intercalation potential of $LiMPO_4$ and $LiMSiO_4$ olivines with M = Fe, Mn, Co, Ni. *Electrochem. Commun.* **6**, 1144–1148 (2004).
21. Van Der Ven, A. & Ceder, G. Lithium diffusion in layered Li_xCoO_2. *Electrochem. Solid-State Lett.* **3**, 301–304 (2000).
22. Ong, S., Wang, L., Kang, B. & Ceder, G. Li–Fe–P–O_2 phase diagram from first principles calculations. *Chem. Mater.* **20**, 1798–1807 (2008).
23. Ong, S. P., Jain, A., Hautier, G., Kang, B. & Ceder, G. Thermal stabilities of delithiated olivine MPO_4 (M = Fe, Mn) cathodes investigated using first principles calculations. *Electrochem. Commun.* **12**, 427–430 (2010).
24. Kang, K., Meng, Y. S., Bréger, J., Grey, C. P. & Ceder, G. Electrodes with high power and high capacity for rechargeable lithium batteries. *Science* **311**, 977–980 (2006).
25. Ong, S. P. *et al.* Phase stability, electrochemical stability and ionic conductivity of the $Li_{10\pm1}MP_2X_{12}$ (M = Ge, Si, Sn, Al or P, and X = O, S or Se) family of superionic conductors. *Energy Environ. Sci.* **12**, 148–156 (2012).
26. Jain, A. *et al.* A high-throughput infrastructure for density functional theory calculations. *Comput. Mater. Sci.* **50**, 2295–2310 (2011).
27. Kim, J. C. *et al.* Synthesis and electrochemical properties of monoclinic $LiMnBO_3$ as a Li intercalation material. *J. Electrochem. Soc.* **158**, A309–A315 (2011).
28. Jain, A. *et al.* A computational investigation of $Li_9M_3(P_2O_7)_3(PO_4)_2$ (M = V, Mo) as cathodes for Li ion batteries. *J. Electrochem. Soc.* **159**, A622–A633 (2012).
29. Ma, X., Hautier, G., Jain, A., Doe, R. & Ceder, G. Improved capacity retention for $LiVO_2$ by Cr substitution. *J. Electrochem. Soc.* **160**, A279–A284 (2012).
30. Hautier, G. *et al.* Novel mixed polyanions lithium-ion battery cathode materials predicted by high-throughput *ab initio* computations. *J. Mater. Chem.* **21**, 17147–17153 (2011).
31. Hautier, G., Fischer, C., Ehrlacher, V., Jain, A. & Ceder, G. Data mined ionic substitutions for the discovery of new compounds. *Inorg. Chem.* **50**, 656–663 (2011).
32. Bergerhoff, G., Hundt, R., Sievers, R. & Brown, I. The inorganic crystal structure data base. *J. Chem. Inf. Comput. Sci.* **23**, 66–69 (1983).
33. Chen, H. *et al.* Carbonophosphates: a new family of cathode materials for Li-ion batteries identified computationally. *Chem. Mater.* **24**, 2009–2016 (2012).
34. Chen, H., Hautier, G. & Ceder, G. Synthesis, computed stability, and crystal structure of a new family of inorganic compounds: carbonophosphates. *J. Am. Chem. Soc.* **134**, 19619–19627 (2012).
35. Chen, H. *et al.* Sidorenkite ($Na_3MnPO_4CO_3$): a new intercalation cathode material for Na-ion batteries. *Chem. Mater.* **25**, 2777–2786 (2013).
36. Huang, W. *et al.* Detailed investigation of $Na_{2.24}FePO_4CO_3$ as a cathode material for Na-ion batteries. *Sci. Rep.* **4**, 4188 (2014).
37. Anasori, B. *et al.* Two-dimensional, ordered, double transition metals carbides (MXenes). *ACS Nano* **9**, 9507–9516 (2015).
38. Schlapbach, L. & Züttel, A. Hydrogen-storage materials for mobile applications. *Nature* **414**, 353–358 (2001).
39. Besenbacher, F. *et al.* Design of a surface alloy catalyst for steam reforming. *Science* **279**, 1913–1915 (1998).
40. Greeley, J., Jaramillo, T. F., Bonde, J., Chorkendorff, I. B. & Nørskov, J. K. Computational high-throughput screening of electrocatalytic materials for hydrogen evolution. *Nat. Mater.* **5**, 909–913 (2006).
This report provided an early example of using density functional theory for 'virtual screening'; here applied to catalytic materials.
41. Medford, A. J. *et al.* From the Sabatier principle to a predictive theory of transition-metal heterogeneous catalysis. *J. Catal.* **328**, 36–42 (2015).
42. Yan, J. *et al.* Materials descriptors for predicting thermoelectric performance. *Energy Environ. Sci.* **8**, 983–994 (2015).
43. Persson, K. A., Waldwick, B., Lazic, P. & Ceder, G. Prediction of solid-aqueous equilibria: scheme to combine first-principles calculations of solids with experimental aqueous states. *Phys. Rev. B* **85**, 235438 (2012).
44. Sun, W., Wolverton, C. & Akbarzadeh, A. First-principles prediction of high-capacity, thermodynamically reversible hydrogen storage reactions based on $(NH_4)_2B_{12}H_{12}$. *Phys. Rev. B* **83**, 064112 (2011).
45. Siegel, D., Wolverton, C. & Ozolins, V. Thermodynamic guidelines for the prediction of hydrogen storage reactions and their application to destabilized hydride mixtures. *Phys. Rev. B* **76**, 134102 (2007).
46. Wolverton, C., Siegel, D. J., Akbarzadeh, A. R. & Ozolins, V. Discovery of novel hydrogen storage materials: an atomic scale computational approach. *J. Phys. Condens. Matter* **20**, 064228 (2008).
47. Alapati, S. V., Johnson, J. K. & Sholl, D. S. Identification of destabilized metal hydrides for hydrogen storage using first principles calculations. *J. Phys. Chem. B* **110**, 8769–8776 (2006).
48. Lu, J., Fang, Z., Choi, Y. & Sohn, H. Potential of binary lithium magnesium nitride for hydrogen storage applications. *J. Phys. Chem. C* **111**, 12129–12134 (2007).
49. Lu, J., Choi, Y. J., Fang, Z. Z. & Sohn, H. Y. Effect of milling intensity on the formation of LiMgN from the dehydrogenation of $LiNH_2$–MgH_2 (1:1) mixture. *J. Power Sources* **195**, 1992–1997 (2010).
50. Osborn, W., Markmaitree, T. & Shaw, L. L. Evaluation of the hydrogen storage behavior of a $LiNH_2 + MgH_2$ system with 1:1 ratio. *J. Power Sources* **172**, 376–378 (2007).
51. Liu, Y. *et al.* Hydrogen storage in a $LiNH_2$–MgH_2 (1:1) system. *Chem. Mater.* **20**, 3521–3527 (2008).
52. Mazin, I. I. Superconductivity gets an iron boost. *Nature* **464**, 183–186 (2010).
53. Kortus, J., Mazin, I. I., Belashchenko, K. D., Antropov, V. P. & Boyer, L. L. Superconductivity of metallic boron in MgB_2. *Phys. Rev. Lett.* **86**, 4656–4659 (2001).
54. Floris, A. *et al.* Superconducting properties of MgB_2 from first principles. *Phys. Rev. Lett.* **94**, 037004 (2005).
55. Mazin, I. I., Singh, D. J., Johannes, M. D. & Du, M. H. Unconventional superconductivity with a sign reversal in the order parameter of $LaFeAsO_{1-x}F_x$. *Phys. Rev. Lett.* **101**, 057003 (2008).
56. Chang, K. J. & Cohen, M. M. L. Structural and electronic properties of the high-pressure hexagonal phases of Si. *Phys. Rev. B* **30**, 5376–5378 (1984).
57. Chang, K. J. *et al.* Superconductivity in high-pressure metallic phases of Si. *Phys. Rev. Lett.* **54**, 2375–2378 (1985).
58. Liu, A. Y. & Cohen, M. L. Electron-phonon coupling in bcc and 9R lithium. *Phys. Rev. B* **44**, 9678–9684 (1991).
59. Neaton, J. B. J. & Ashcroft, N. W. Pairing in dense lithium. *Nature* **400**, 141–144 (1999).
60. Christensen, N. E. & Novikov, D. L. Predicted superconductive properties of lithium under pressure. *Phys. Rev. Lett.* **86**, 1861–1864 (2001).
61. Shimizu, K., Ishikawa, H., Takao, D., Yagi, T. & Amaya, K. Superconductivity in compressed lithium at 20 K. *Nature* **419**, 597–599 (2002).
62. Struzhkin, V. V., Eremets, M. I., Gan, W., Mao, H.-k. & Hemley, R. J. Superconductivity in dense lithium. *Science* **298**, 1213–1215 (2002).
63. Deemyad, S. & Schilling, J. S. Superconducting phase diagram of Li metal in nearly hydrostatic pressures up to 67 GPa. *Phys. Rev. Lett.* **91**, 167001 (2003).
64. Kolmogorov, A. N. *et al.* New superconducting and semiconducting Fe-B compounds predicted with an *ab initio* evolutionary search. *Phys. Rev. Lett.* **105**, 217003 (2010).
65. Gou, H. *et al.* Discovery of a superhard iron tetraboride superconductor. *Phys. Rev. Lett.* **111**, 157002 (2013).
66. Li, Y., Hao, J., Liu, H., Li, Y. & Ma, Y. The metallization and superconductivity of dense hydrogen sulfide. *J. Chem. Phys.* **140**, 174712 (2014).
67. Drozdov, A. P., Eremets, M. I., Troyan, I. A., Ksenofontov, V. & Shylin, S. I. Conventional superconductivity at 203 kelvin at high pressures in the sulfur hydride system. *Nature* **525**, 73–76 (2015).
68. Ashcroft, N. Hydrogen dominant metallic alloys: high temperature superconductors? *Phys. Rev. Lett.* **92**, 187002 (2004).
69. Eremets, M. I., Troyan, I. A., Medvedev, S. A., Tse, J. S. & Yao, Y. Superconductivity in hydrogen dominant materials: silane. *Science* **319**, 1506–1509 (2008).
70. Pickard, C. J. & Needs, R. J. High-pressure phases of silane. *Phys. Rev. Lett.* **97**, 045504 (2006).
71. Hanfland, M., Proctor, J. E., Guillaume, C. L., Degtyareva, O. & Gregoryanz, E. High-pressure synthesis, amorphization, and decomposition of silane. *Phys. Rev. Lett.* **106**, 095503 (2011).
72. Richard, C. *et al. Renewable energy data book* (US Department of Energy, 2013).
73. Green, M. A., Emery, K., Hishikawa, Y., Warta, W. & Dunlop, E. D. Solar cell efficiency tables (version 45). *Prog. Photovoltaics* **23**, 1–9 (2015).
74. Yu, L. & Zunger, A. Identification of potential photovoltaic absorbers based on first-principles spectroscopic screening of materials. *Phys. Rev. Lett.* **108**, 068701 (2012).
75. Yu, L., Kokenyesi, R. S., Keszler, D. A. & Zunger, A. Inverse design of high absorption thin-film photovoltaic materials. *Adv. Energy Mater.* **3**, 43–48 (2013).
76. Levi, B. G. Nobel prize in Chemistry salutes the discovery of conducting polymers. *Phys. Today* **53**, 19–22 (2000).
77. Davis, W., Svec, W., Ratner, M. & Wasielewski, M. Molecular-wire behaviour in *p*-phenylenevinylene oligomers. *Nature* **396**, 60–63 (1998).
78. Roncali, J. Conjugated poly(thiophenes) — synthesis, functionalization, and applications. *Chem. Rev.* **92**, 711–738 (1992).
79. Peters, C. H. *et al.* High efficiency polymer solar cells with long operating lifetimes. *Adv. Energy Mater.* **1**, 491–494 (2011).
80. Mühlbacher, D. *et al.* High photovoltaic performance of a low-bandgap polymer. *Adv. Mater.* **18**, 2884–2889 (2006).
81. Heeger, A. J. Semiconducting polymers: the third generation. *Chem. Soc. Rev.* **39**, 2354–2371 (2010).
82. Cohen, A. J., Mori-Sánchez, P. & Yang, W. Insights into current limitations of density functional theory. *Science* **321**, 792–794 (2008).
83. Bedard-Hearn, M. J., Sterpone, F. & Rossky, P. J. Nonadiabatic simulations of exciton dissociation in poly-*p*-phenylenevinylene oligomers. *J. Phys. Chem. A* **114**, 7661–7670 (2010).
84. Hannewald, K. *et al.* Theory of polaron bandwidth narrowing in organic molecular crystals. *Phys. Rev. B* **69**, 075211 (2004).
85. Shin, Y. & Lin, X. Modeling photoinduced charge transfer across π-conjugated heterojunctions. *J. Phys. Chem. C* **117**, 12432–12437 (2013).
86. Hachmann, J. *et al.* The Harvard Clean Energy Project: large-scale computational screening and design of organic photovoltaics on the world community grid. *J. Phys. Chem. Lett.* **2**, 2241–2251 (2011).
87. Körzdörfer, T. & Brédas, J.-L. Organic electronic materials: recent advances in the DFT description of the ground and excited states using tuned range-separated hybrid functionals. *Acc. Chem. Res.* **47**, 3284–3291 (2014).
88. Sokolov, A. N. *et al.* From computational discovery to experimental characterization of a high hole mobility organic crystal. *Nat. Commun.* **2**, 437 (2011).
89. Blouin, N. *et al.* Toward a rational design of poly(2,7carbazole) derivatives for solar cells. *J. Am. Chem. Soc.* **130**, 732–742 (2008).
90. Shin, Y., Liu, J., Quigley, J. J., Luo, H. & Lin, X. Combinatorial design of copolymer donor materials for bulk heterojunction solar cells. *ACS Nano* **8**, 6089–6096 (2014).

91. Hautier, G., Miglio, A., Ceder, G., Rignanese, G.-M. & Gonze, X. Identification and design principles of low hole effective mass p-type transparent conducting oxides. *Nat. Commun.* **4**, 2292 (2013).
92. Bathia, A. *et al.* High-mobility bismuth-based transparent p-type oxide from high-throughput material screening. Preprint at http://arXiv.org/abs/1412.4429 (2014).
93. Yan, F. *et al.* Design and discovery of a novel half-Heusler transparent hole conductor made of all-metallic heavy elements. *Nat. Commun.* **6**, 7308 (2015).
94. Tritt, T. & Subramanian, M. Thermoelectric materials, phenomena, and applications: a bird's eye view. *MRS Bull.* **31**, 188–198 (2006).
95. Pei, Y. *et al.* Convergence of electronic bands for high performance bulk thermoelectrics. *Nature* **473**, 66–69 (2011).
96. Qiu, B. *et al.* First-principles simulation of electron mean-free-path spectra and thermoelectric properties in silicon. *Europhys. Lett.* **109**, 57006 (2015).
97. Madsen, G. K. H. Automated search for new thermoelectric materials: the case of LiZnSb. *J. Am. Chem. Soc.* **128**, 12140–12146 (2006).
This paper established the general methodology for computational screening of thermoelectric materials, which has inspired several extensions and further studies.
98. Toberer, E. S., May, A. F., Scanlon, C. J. & Snyder, G. J. Thermoelectric properties of p-type LiZnSb: assessment of *ab initio* calculations. *J. Appl. Phys.* **105**, 063701 (2009).
99. Gorai, P., Parilla, P., Toberer, E. S. & Stevanovic, V. Computational exploration of the binary A_1B_2 chemical space for thermoelectric performance. *Chem. Mater.* **27**, 6213–6221 (2015).
100. Wang, S., Wang, Z., Setyawan, W., Mingo, N. & Curtarolo, S. Assessing the thermoelectric properties of sintered compounds via high-throughput *ab initio* calculations. *Phys. Rev. X* **1**, 021012 (2011).
101. Zhu, H. *et al.* Computational and experimental investigation of $TmAgTe_2$ and XYZ_2 compounds, a new group of thermoelectric materials identified by first-principles high-throughput screening. *J. Mater. Chem. C* **3**, 10554–10565 (2015).
102. Sharma, V. *et al.* Rational design of all organic polymer dielectrics. *Nat. Commun.* **5**, 4845 (2014).
103. Pilania, G. *et al.* New group IV chemical motifs for improved dielectric permittivity of polyethylene. *J. Chem. Inf. Model.* **53**, 879–886 (2013).
104. Wang, C. C., Pilania, G. & Ramprasad, R. Dielectric properties of carbon-, silicon-, and germanium-based polymers: a first-principles study. *Phys. Rev. B* **87**, 035103 (2013).
105. Ma, R. *et al.* Rational design and synthesis of polythioureas as capacitor dielectrics. *J. Mater. Chem. A* **3**, 14845–14852 (2015).
106. Bentien, A., Madsen, G., Johnsen, S. & Iversen, B. Experimental and theoretical investigations of strongly correlated $FeSb_{2-x}Sn_x$. *Phys. Rev. B* **74**, 205105 (2006).
107. Bentien, A., Johnsen, S., Madsen, G. K. H., Iversen, B. B. & Steglich, F. Colossal Seebeck coefficient in strongly correlated semiconductor $FeSb_2$. *Europhys. Lett.* **80**, 17008 (2007).
108. Kojima, A., Teshima, K., Shirai, Y. & Miyasaka, T. Organometal halide perovskites as visible-light sensitizers for photovoltaic cells. *J. Am. Chem. Soc.* **131**, 6050–6051 (2009).
109. Yin, W.-J., Yang, J.-H., Kang, J., Yan, Y. & Wei, S.-H. Halide perovskite materials for solar cells: a theoretical review. *J. Mater. Chem. A* **3**, 8926–8942 (2015).
110. Perdew, J. P., Ruzsinszky, A., Constantin, L. A., Sun, J. & Csonka, G. I. Some fundamental issues in ground-state density functional theory: a guide for the perplexed. *J. Chem. Theory Comput.* **5**, 902–908 (2009).
111. Burke, K. Perspective on density functional theory. *J. Chem. Phys.* **136**, 150901 (2012).
112. Cohen, A. J., Mori-Sanchez, P. & Yang, W. Challenges for density functional theory. *Chem. Rev.* **112**, 289–320 (2012).
113. Fonseca Guerra, C., Snijders, J. G., Te Velde, G. & Baerends, E. J. Towards an order-*N* DFT method. *Theor. Chem. Acc.* **99**, 391–403 (1998).
114. Baroni, S., Gironcoli, S. D., Corso, A. D. & Giannozzi, P. Phonons and related crystal properties from density functional perturbation theory. *Rev. Mod. Phys.* **73**, 515 (2001).
115. Sanchez, J. M., Ducastelle, F. & Gratias, D. Generalized cluster description of multicomponent systems. *Phys. A* **128**, 334–350 (1984).
116. Runge, E. & Gross, E. K. U. Density functional theory for time-dependent systems. *Phys. Rev. Lett.* **52**, 997–1000 (1984).
117. Petersilka, M., Gossmann, U. & Gross, E. Excitation energies from time-dependent density functional theory. *Phys. Rev. Lett.* **76**, 1212–1215 (1996).
118. Hedin, L. New method for calculating the one-particle Green's function with application to the electron-gas problem. *Phys. Rev.* **139**, A796–A823 (1965).
119. Salpeter, E. & Bethe, H. A relativistic equation for bound-state problems. *Phys. Rev.* **84**, 1232–1242 (1951).
120. Klimeš, J. & Michaelides, A. Perspective: advances and challenges in treating van der Waals dispersion forces in density functional theory. *J. Chem. Phys.* **137**, 120901 (2012).
121. Carter, E. A. Challenges in modeling materials properties without experimental input. *Science* **321**, 800–803 (2008).
122. Jones, G., Bligaard, T., Abild-Pedersen, F. & Nørskov, J. K. Using scaling relations to understand trends in the catalytic activity of transition metals. *J. Phys. Condens. Matter* **20**, 064239 (2008).
123. Nørskov, J. K., Abild-Pedersen, F., Studt, F. & Bligaard, T. Surface chemistry special feature: Density functional theory in surface chemistry and catalysis. *Proc. Natl Acad. Sci. USA* **108**, 937–943 (2011).
124. Jain, A. *et al.* Commentary: The Materials Project: a materials genome approach to accelerating materials innovation. *APL Mater.* **1**, 011002 (2013).
Introduction of the Materials Project, today's most popular searchable database of density functional theory calculations used by both experimentalists and theorists.
125. Curtarolo, S. *et al.* AFLOWLIB.ORG: a distributed materials properties repository from high-throughput *ab initio* calculations. *Comput. Mater. Sci.* **58**, 227–235 (2012).
126. Saal, J. E., Kirklin, S., Aykol, M., Meredig, B. & Wolverton, C. Materials design and discovery with high-throughput density functional theory: the open quantum materials database (OQMD). *JOM* **65**, 1501–1509 (2013).
127. Landis, D. D. *et al.* The computational materials repository. *Comput. Sci. Eng.* **14**, 51–57 (2012).
128. Oganov, A. R. & Valle, M. How to quantify energy landscapes of solids. *J. Chem. Phys.* **130**, 104504 (2009).
129. Maddox, J. Crystals from first principles. *Nature* **335**, 201 (1988).
130. Pickard, C. J. & Needs, R. J. *Ab initio* random structure searching. *J. Phys. Condens. Matter* **23**, 053201 (2011).
131. Oganov, A. R. & Glass, C. W. Crystal structure prediction using *ab initio* evolutionary techniques: principles and applications. *J. Chem. Phys.* **124**, 244704 (2006).
132. Curtarolo, S., Morgan, D., Persson, K., Rodgers, J. & Ceder, G. Predicting crystal structures with data mining of quantum calculations. *Phys. Rev. Lett.* **91**, 135503 (2003).
133. Fischer, C. C., Tibbetts, K. J., Morgan, D. & Ceder, G. Predicting crystal structure by merging data mining with quantum mechanics. *Nat. Mater.* **5**, 641–646 (2006).
134. Hautier, G., Fischer, C. C., Jain, A., Mueller, T. & Ceder, G. Finding nature's missing ternary oxide compounds using machine learning and density functional theory. *Chem. Mater.* **22**, 3762–3767 (2010).
135. Meredig, B. *et al.* Combinatorial screening for new materials in unconstrained composition space with machine learning. *Phys. Rev. B* **89**, 094104 (2014).
136. Meredig, B. & Wolverton, C. A hybrid computational experimental approach for automated crystal structure solution. *Nat. Mater.* **12**, 123–127 (2013).
137. Pickard, C. J. & Needs, R. J. Highly compressed ammonia forms an ionic crystal. *Nat. Mater.* **7**, 775–779 (2008).
138. Ninet, S. *et al.* Experimental and theoretical evidence for an ionic crystal of ammonia at high pressure. *Phys. Rev. B* **89**, 174103 (2014).
139. Palasyuk, T. *et al.* Ammonia as a case study for the spontaneous ionization of a simple hydrogen-bonded compound. *Nat. Commun.* **5**, 3460 (2014).
140. Ma, Y. *et al.* Transparent dense sodium. *Nature* **458**, 182–185 (2009).
141. Fix, T., Sahonta, S.-L., Garcia, V., MacManus-Driscoll, J. L. & Blamire, M. G. Structural and dielectric properties of $SnTiO_3$, a putative ferroelectric. *Cryst. Growth Des.* **11**, 1422–1426 (2011).
142. Gautier, R. *et al.* Prediction and accelerated laboratory discovery of previously unknown 18-electron ABX compounds. *Nat. Chem.* **7**, 308–316 (2015).
143. Bron, P. *et al.* $Li_{10}SnP_2S_{12}$: an affordable lithium superionic conductor. *J. Am. Chem. Soc.* **135**, 15694–15697 (2013).
144. Studt, F. *et al.* Discovery of a Ni-Ga catalyst for carbon dioxide reduction to methanol. *Nat. Chem.* **6**, 320–324 (2014).
145. Cole, J. M. *et al.* Data mining with molecular design rules identifies new class of dyes for dye-sensitised solar cells. *Phys. Chem. Chem. Phys.* **16**, 26684–26690 (2014).

Acknowledgements
This work was intellectually led by the Materials Project supported by the US Department of Energy Office of Science, Office of Basic Energy Sciences Department under Contract No. DE-AC02-05CH11231. Y.S. thanks the Battery Materials Research Program under the Assistant Secretary for Energy Efficiency and Renewable Energy, Office of Vehicle Technologies of the US Department of Energy.

Competing interests
The authors declare no competing interests.